JACS
JOURNAL OF THE AMERICAN CHEMICAL SOCIETY
Article
pubs.acs.org/JACS

General Rules for Selective Growth of Enriched Semiconducting Single Walled Carbon Nanotubes with Water Vapor as in Situ Etchant

Weiwei Zhou, Shutong Zhan, Lei Ding, and Jie Liu*

Department of Chemistry, Duke University, Durham, North Carolina 27708, United States

Supporting Information

ABSTRACT: The presence of metallic nanotubes in as-grown single walled carbon nanotubes (SWNTs) is the major bottleneck for their applications in field-effect transistors. Herein, we present a method to synthesize enriched, semiconducting nanotube arrays on quartz substrate. It was discovered that introducing appropriate amounts of water could effectively remove the metallic nanotubes and significantly enhance the density of SWNT arrays. More importantly, we proposed and confirmed that the high growth selectivity originates from the etching effect of water and the difference in the chemical reactivities of metallic and semiconducting nanotubes. Three important rules were summarized for achieving a high selectivity in growing semiconducting nanotubes by systematically investigating the relationship among water concentration, carbon feeding rate, and the percentage of semiconducting nanotubes in the produced SWNT arrays. Furthermore, these three rules can be applied to the growth of random SWNT networks on silicon wafers.

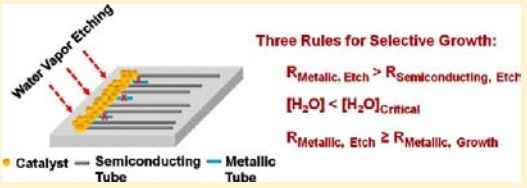

INTRODUCTION

In the research field that is constantly searching for electronic devices beyond silicon, the carbon nanotube has been a leading candidate for many years since its discovery.[1,2] In recent years, another carbon-based material, graphene, is becoming an actively studied alternative for future electronics and has shown great promise.[3] The competition between these two carbon-based materials is attracting attention from many research groups. More recently, experimental and theoretical works have shown that, at least in high-frequency electronic devices, aligned carbon nanotube arrays outperform devices made from graphene.[4,5] As a result, parallel single walled carbon nanotube (SWNT) arrays on substrates have attracted more attention than random SWNTs due to their great potential in RF devices where impedance matching becomes important.[6−9] Using a SWNT array instead of a single tube as the device channel material has made obvious performance improvements in the on-driving current, the device-to-device consistency, and the compatibility with existing Si fabrication technology.[10] Nevertheless, the presence of metallic nanotubes in the SWNT arrays still causes the poor on/off ratios in SWNT array-based field-effect transistors (FETs). Therefore, one of the most significant challenges is selective preparation of semiconducting SWNTs on target substrates.

Recently, some research efforts focused on using a pure semiconducting SWNT solution to achieve high on/off ratios.[11−13] Studies show the good on/off ratio could be obtained only in the long-channel FETs along with using SWNT solution with ultrahigh purity of semiconducting SWNTs.[11−13] However, when the channel length is long, the on-driving current density would be significantly reduced. Moreover, the mobility of the FETs made from the purified SWNT solution is at least an order of magnitude below that of the FETs based on the horizontally aligned SWNT arrays synthesized by chemical vapor deposition (CVD) method due to the low-degree alignment, short length of SWNTs, and high-density defects on the SWNT surface created by purified processes.[14]

A more feasible approach is to directly grow high-quality semiconducting SWNTs on suitable substrates with well-controlled growth directions by the CVD method.[15,16] A methanol/ethanol CVD method has been established earlier in our lab to achieve the growth of perfectly aligned SWNTs arrays with over 95% nanotubes being semiconducting on Y-cut quartz substrates.[16] However, the mechanism is still far from clear. On the basis of the experimental observations and discussions published by us[16] and other groups,[17,18] a possible hypothesis is that the selectivity of growing semiconducting SWNTs in the methanol/ethanol CVD method could originate from the etching of hydroxyl groups and chemical reactivity difference of metallic and semiconducting nanotubes with hydroxyl groups. If simply assuming that the etching rate is decided by etchant concentration and the growing rate is decided by carbon feeding rate, an optimal etchant concentration and carbon feeding rate would be found, where only semiconducting nanotubes can grow and not be etched while very few metallic nanotubes can grow and easily be removed according to experimental observations. Therefore, it is crucial to systematically investigate the relationships of etchant concentration and carbon feeding rate with the distribution of SWNT electronic types for exclusively growing semiconducting nanotubes and verify the hypothesized mechanism. However, in the methanol/ethanol CVD method, methanol and ethanol not

Received: April 23, 2012
Published: August 8, 2012

   dx.doi.org/10.1021/ja3038992 | J. Am. Chem. Soc. 2012, 134, 14019−14026

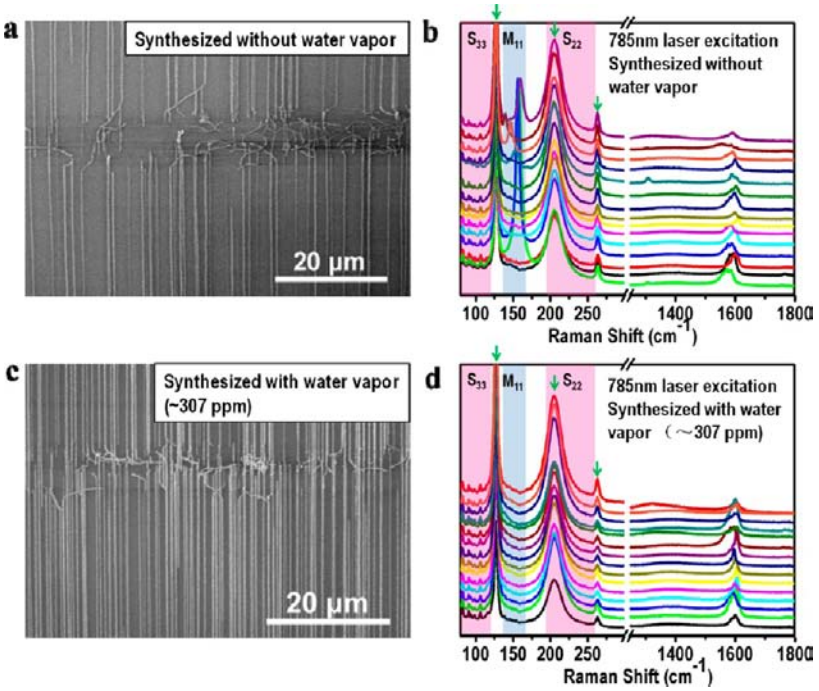

Figure 1. SWNT arrays grown on quartz synthesized with or without water vapor by the CVD method. SEM image (a) and Raman spectra (b) of the SWNT array sample synthesized using a H_2 flow at 280 sccm and an Ar flow through ethanol bubbler at 80 sccm. SEM image (c) and Raman spectra (d) of the SWNT array sample synthesized using a H_2 flow at 330 sccm, an Ar flow through ethanol bubbler at 80 sccm, and another Ar flow through water bubbler at 20 sccm (water vapor concentration: ~307 ppm). The laser excitation wavelength of Raman spectroscopy is 785 nm. The regions corresponding to semiconducting transitions are labeled as $S_{11,22}$ and $S_{33,44}$ (shaded pink), and the first-order metallic transition is labeled as M_{11} (shaded blue). The peaks at 128, 205, and 264 cm^{-1} indicated by green arrows originate from quartz substrates. The small peaks between 80 and 120 cm^{-1} in (b) and (d) originate from the 785 nm laser. The spectra were collected at 15 spots for each sample.

only provide the hydroxyl group but also are the carbon feeding source. In order to further clarify the mechanism, we designed a new series of experiments using carbon-free etchant.

A trace amount of oxygen has been shown to selectively etch metallic nanotubes in the floating catalyst CVD method.[18] However, as a strong oxidizing reagent, oxygen concentration is difficult to control in the CVD process because it easily reacts with all carbonaceous species at SWNT growth temperature. Compared with oxygen, water vapor has a much weaker oxidizing ability, and its concentration in the CVD chamber can be delicately controlled by the flow rate of carrier gas through a bubbler. Therefore, in this study, we developed a water vapor-assisted CVD method to selectively grow semiconducting SWNTs on quartz substrates. Systematic experiments have been performed by varying the carrier gas flow through a water bubbler and using a fixed carrier gas flow through an ethanol bubbler. It is discovered that a high selectivity of semiconducting SWNTs can be achieved on quartz substrate when an optimal water concentration and a low carbon feeding rate were used. In the meantime, the growth efficiency of SWNTs has shown a significant enhancement on both quartz and silicon substrates by the addition of appropriate amounts of water vapor, which is in accord with the "super-growth" method for growing vertically aligned SWNTs.[19,20] At a higher carbon feeding rate, the percentages of semiconducting nanotubes as estimated from electrical measurement varied with the concentration of water vapor. However, the highest purity of semiconducting nanotubes in the sample synthesized at a high carbon feeding rate is lower than those using the low carbon feeding rate, which indicates that the etchant concentration and carbon feeding rate both play important roles in determining the distribution of SWNT electronic types in the surface growth of SWNTs by the CVD method.

EXPERIMENTAL SECTION

Growth of Horizontally Aligned SWNT Arrays on Quartz Wafers. A 1.0 mM $CuCl_2$/poly vinylpyrrolidone ethanol solution was used as catalyst precursor and patterned on Y-cut quartz wafers (purchased from http://www.universitywafer.com) first following a procedure previously described by us.[21] The quartz wafers were calcined at 775 °C in air for 15 min to remove polymer and form Cu_xO_y nanoparticles. After the wafers cooled down to room temperature, the furnace was heated to 775 °C, and the wafers dwelt at 775 °C for 15 min in H_2 atmosphere, followed by the CVD growth of SWNTs at 900 °C. A mixed gas of H_2 at ~330 or ~280 sccm, one Ar flow through an ethanol bubbler at ~80 sccm, and another Ar flow through a water bubbler at varied flow rates were introduced into the system. Both bubblers were soaked in the mixture of ice/water and kept at the temperature of 0−2 °C. After 15 min of growth, the Ar gas channel was terminated, and the furnace was cooled down to room temperature while protected by H_2.

Growth of Random SWNT Networks on Silicon Wafers. A 0.1 mM $FeCl_3$/poly vinylpyrrolidone ethanol solution was used as catalyst precursors and dropped onto the silicon wafer surface and dried in air. After loading the catalyst, the silicon wafers with 500 nm of silicon oxide layer (purchased from Silicon Quest International, Inc.) were calcined at 750 °C in air for 5 min to remove polymer and form Fe_xO_y nanoparticles. After cooled down to room temperature, the furnace was ramped to 900 °C and dwelt at 900 °C for 5 min in H_2 atmosphere for reducing Fe_xO_y nanoparticles to Fe nanoparticles, followed by the CVD growth of SWNTs at 900 °C. A mixed gas of H_2 at ~130 sccm, one Ar flow through an ethanol bubbler at ~105 sccm, and another Ar flow through a water bubbler at varied flow rates were introduced into the system. Both bubblers were soaked in the mixture of ice/water and kept at the temperature of 0−2 °C. After 15 min of

dx.doi.org/10.1021/ja3038992 | J. Am. Chem. Soc. 2012, 134, 14019−14026

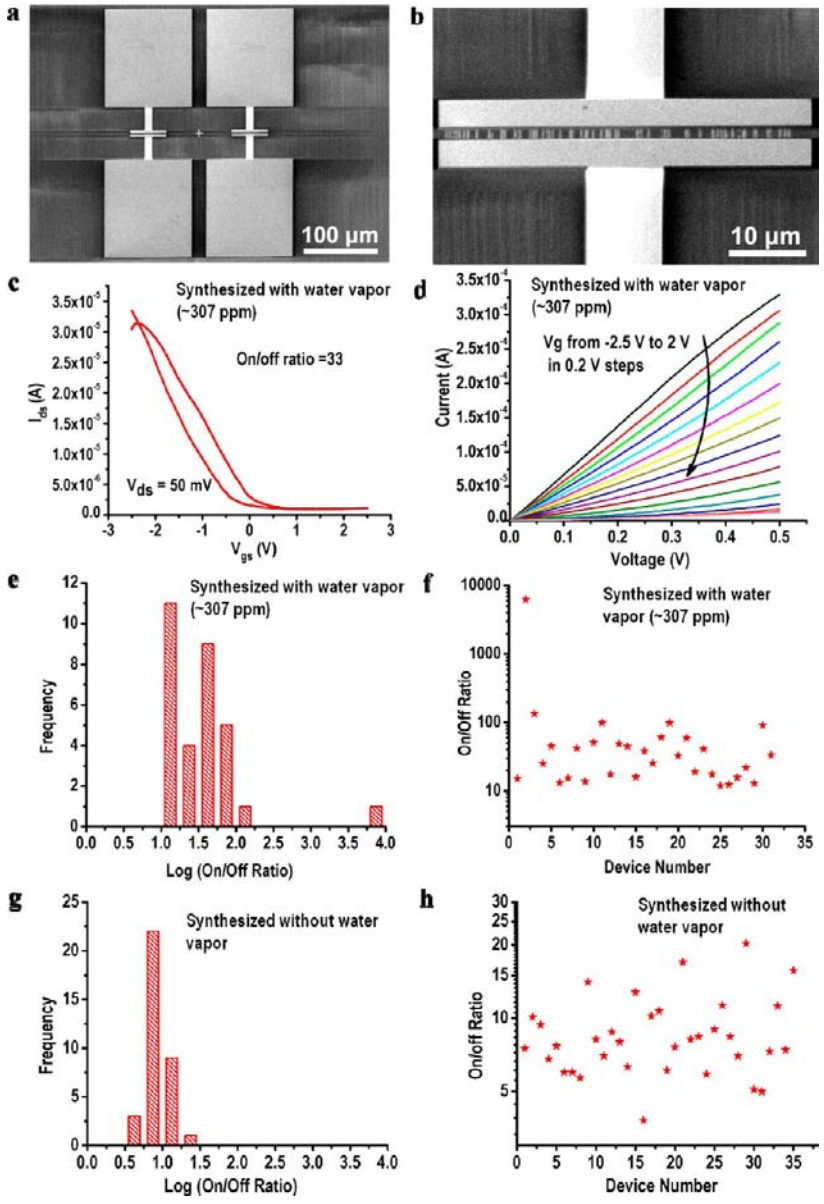

Figure 2. On/off ratio measurement results of the SWNT array samples synthesized with and without water vapor, respectively. SEM images (a,b) and transfer (c) and output characteristics (d) of a representative device fabricated on an SWNT array sample synthesized with water vapor. Histograms of on/off ratio distributions of the TFT devices based on the SWNT array samples synthesized with (e) and without water vapor (g). Display of on/off ratios of all TFT devices based on the SWNT array samples synthesized with (f) and without water vapor (h).

growth, Ar gas channel was terminated, and the furnace was cooled down to room temperature while protected by H_2.

Fabrication and Measurement of Thin Film Transistor Devices Using Ionic Liquid Gating. Thin film transistor (TFT) devices with channel length of 2 μm and width of 50 μm were patterned by a standard e-beam lithography (EBL) process. Ti (1.0 nm)/Pd (20 nm)/Au (40 nm) were deposited by e-beam evaporation, followed by a lift-off process to form contact electrodes. Another EBL process and O_2 plasma etching were used to remove the shorting nanotubes outside the device channel region. The ionic liquid of butyltrimethylammonium bis(trifluoromethylsulfonyl)imide was used for gating. The source-drain bias was 50 mV. A Keithley 4200-SCS semiconductor characterization system was used for measuring the electrical characteristics.

Characterization. A scanning electron microscope (SEM, FEI XL30 S-FEG, operated at 1 or 1.5 kV), an atomic force microscope (AFM, Digital Instruments Multi-Mode SPM Nanoscope IIIa, operated in tapping-mode), a high-resolution transmission electron microscope (HRTEM, Tecnai F20 FEG-TEM, operated at 200 kV) and a micro-Raman spectroscope (Horiba Jobin Yvon LabRam ARAMIS) were used to characterize the produced SWNTs. The excitation wavelengths of micro-Raman we used are 633 and 785 nm. For HRTEM characterization, the samples were transferred from quartz wafers onto the Cu grids.

■ RESULTS AND DISCUSSION

Synthesis of Enriched Semiconducting SWNT Arrays on Quartz Wafer by Introducing an Appropriate Amount of Water Vapor. In a typical growth process, a flow of H_2 (330 sccm) and Ar (80 sccm through an ethanol bubbler and 20 sccm through a water bubbler) was introduced at the CVD growth temperature of 900 °C for 15 min. The water vapor concentration in the CVD chamber is calculated to be ~307 ppm under these conditions (see Supporting Information [SI]). As shown in Figure 1c, a uniform SWNT array with the density of 1−2 SWNT/μm was synthesized.

dx.doi.org/10.1021/ja3038992 | J. Am. Chem. Soc. 2012, 134, 14019−14026

Raman spectroscopy, as a powerful tool of revealing the detailed structure of carbon nanotubes, was used to estimate the diameter distribution of nanotubes and distinguish metallic and semiconducting nanotubes in our samples. According to the Kataura plot,[22] only radical breath mode (RBM) peaks of semiconducting tubes were detected under the excitation of 633 nm laser (see SI, Figure S1), and the diameter of SWNT in the sample varies from 1.6 to 2.1 nm calculated from the empirical equation of $\omega = 248/d_t$[22] where ω is a RBM shift and d_t is a nanotube diameter. No RBM peak was found when a 785 nm laser was used (Figure 1d), indicating the presence of no or few metallic nanotubes with the diameter from 1.5 to 1.9 nm in the sample corresponding to the pink region in Raman spectra (Figure 1d). On the other hand, the barely noticeable D band at the high-frequency region of Raman spectra means that water vapor with such a small concentration does not cause structural defects in SWNTs.

Raman characterization provides strong evidence that semiconducting nanotubes preferentially grow when introducing water vapor into an ethanol CVD process. However, RBM signals only can be collected from the carbon nanotube species that can show resonance with the excitation laser lines. In addition, RBM signals of the large-diameter nanotubes, especially with the diameters larger than 2 nm, are hardly observed in the Raman spectrum. In fact, atomic force microscopy (AFM) results show the diameter distribution of SWNTs is from 1.0 to 4.9 nm and the average diameter is 2.6 nm, which is further confirmed by high-resolution transmission microscope (HRTEM) characterization (see SI, Figure S2). Therefore, it is necessary to perform electrical characterizations of the TFTs fabricated from the as-grown SWNT array synthesized with water vapor for further confirmation of the enrichment of semiconducting nanotubes. Typically, the fabricated TFT has a channel length of 2 μm and width of 50 μm (Figure 2a,b). Ionic liquid was used for top-gating,[23] and 50 mV was used for source-drain bias voltage. The ionic liquid used as the gate dielectric is more efficient than a conventional solid gate since a narrow electric double layer is formed at the interface of liquid and channel material, which provides a large capacitance.[24,25] In a representative device (see SI, Figure S3), a Pt electrode used as gate electrode was immersed in a small drop of ionic liquid. As shown in Figure 2e,f, 31 devices were fabricated, and the median value of on/off ratio is 32.5, with the minimum value as 11.8 and maximum value reaching an order of 10^3. The transfer and output characteristics of a representative device were shown in Figure 2c,d. To further confirm the reliability and reproducibility of the result, we measured more than 100 devices on three different samples synthesized using the identical CVD conditions, and consistent results were observed. Assuming all carbon nanotubes have similar on-state resistivity, the percentage of semiconducting nanotubes can be estimated by the formula of $R = 1/(1 - P_s)$, where R is the on/off ratio of a device and P_s is the percentage of semiconducting nanotubes. Thus, for the median on/off ratio of ~32.5, ~97% semiconducting nanotubes are expected in the SWNT arrays synthesized with ~307 ppm water vapor. In fact, it has been reported that metallic tubes often carry higher current than semiconducting tubes when they have similar diameters.[13,26] Thus, the real percentage of semiconducting nanotubes could be higher than ~97%.

To demonstrate more clearly the effect of water on the growth of horizontally aligned SWNT array on a quartz substrate, a SWNT array synthesized under the same CVD conditions but without adding water vapor into the growth process was originally planned for control experiments. However, we found that SWNTs barely grew under this CVD condition (see SI, Figure S4). Therefore, it is obvious that introducing water vapor can greatly enhance the growth efficiency of horizontally aligned SWNTs. In order to obtain a uniform SWNT array under conditions without water vapor, we altered the flow rate of H_2 to obtain a higher carbon feeding rate. When the H_2 flow rate was decreased to 280 sccm, an SWNT array with a density of 0.5−1 SWNTs/μm was synthesized (Figure 1a). In contrast to the sample synthesized with water vapor, Raman spectra of the sample synthesized without water vapor show many RBM peaks from metallic tube resonance under the excitation wavelength of the 785 nm laser (Figure 1b). At the same time, we measured the on/off ratio of fabricated devices and found that the median value is 8 (Figure 2g,h), and only ~29% devices have an on/off ratio larger than 10. Therefore, it is demonstrated here that the high selectivity of growing semiconducting nanotubes results from introducing a suitable amount of water. Moreover, no significant change of on-state current was observed (see SI, Figure S5), indicating that there are no obvious structural defects introduced which can result in the decrease of the device conductance. Compared with the sample made without water vapor, there are more devices in Figure S5a (SI) showing low on-state currents, which is due to a high percentage of semiconducting nanotubes in the device channel.

It should be noted that feeding more water vapor than an optimal amount causes a dramatic density decrease of SWNT array. As shown in SI, Figure S4e,f, the density of SWNTs was only ~0.2 SWNT/μm when Ar flow through water was increased from 20 sccm (water concentration ~307 ppm) to 30 sccm (water concentration ~450 ppm), and there are many short SWNT fragments in Figure S4f (SI), indicating that many horizontally aligned SWNTs were etched by excessive water. Moreover, on/off ratio measurement results show no obvious selectivity in this sample (see SI, Figure S6). Therefore, the experimental results show that water vapor concentration can greatly affect the electronic type distribution and density of SWNTs synthesized by this water/ethanol CVD method.

Mechanism of Selective Growth of Semiconducting Nanotubes. To further investigate the oxidizing property of water vapor, we also annealed as-grown aligned SWNT arrays grown using pure ethanol at 900 °C for 15 min under a water vapor concentration of 307 ppm. SEM and Raman characterizations show that there is no noticeable change of horizontally aligned SWNTs after water vapor treatment, but most of the random SWNTs in the catalyst area disappeared (see SI, Figure S7), indicating that the horizontally aligned SWNTs are stable and barely removed by postsynthesis etching under such a low water concentration, whereas the random nanotubes are easily attacked by water vapor which might be due to the existence of catalyst particles.[27,28] The result of postsynthesis oxidation experiment means that the high selectivity of growing semiconducting nanotubes only can be realized during the CVD growth process. In a CVD growth process, the carbon nanotubes nucleate and grow out from catalyst particles, while simultaneously some of them are etched by oxidants. The semiconducting tubes are believed to be more stable than metallic tubes; i.e. the metallic tubes are preferentially etched by water vapor under a certain condition.[16,29] Moreover, the etching effect exclusively happened in the catalyst area, which

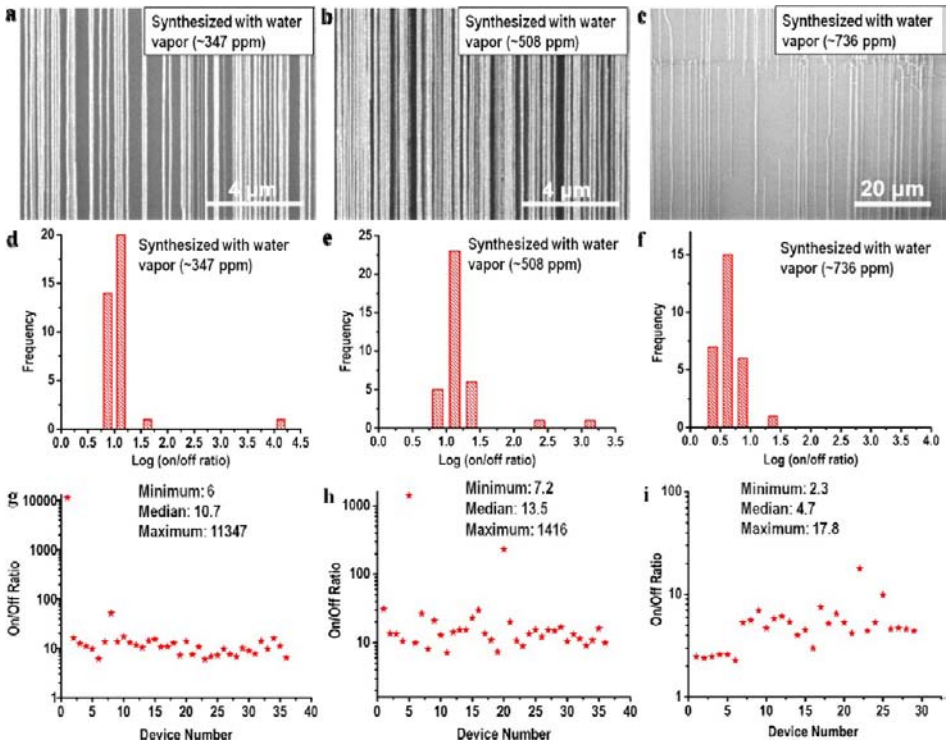

Figure 3. Water effect on the growth of the SWNT array samples synthesized on quartz by using a higher carbon feeding rate. SEM images of the SWNT array samples synthesized with the water vapor concentration of ~347 ppm (Ar flow through water bubbler at 20 sccm) (a), ~508 ppm (Ar flow through water bubbler at 30 sccm) (b), and ~736 ppm (Ar flow through water bubbler at 45 sccm) (c). The three samples were synthesized using a H_2 flow of 280 sccm and another Ar flow through ethanol bubbler of 80 sccm. Histograms of on/off ratio distributions of the TFT devices based on the SWNT array samples synthesized with the water vapor concentration of ~347 (d), ~508 (e), and ~736 ppm (f). Display of on/off ratios of all TFT devices based the SWNT array samples synthesized with the water vapor concentration of ~347 (g), ~508 (h), and ~736 ppm (i).

indicates that the preferentially etching only occurs around/on the catalyst nanoparticles.

Thus, one of the essential factors for achieving high selectivity is to choose a suitable concentration of water vapor that makes the etching rate of metallic tubes larger than that of semiconducting tubes. We can simply describe this rule as $R_{m,ETCH} > R_{s,ETCH}$, where $R_{m,ETCH}$ is the etching rate of metallic tubes and $R_{s,ETCH}$ is the etching rate of semiconducting tubes. Both of them are determined by the water vapor concentration $[H_2O]$. Additionally, $[H_2O]$ should be lower than the critical concentration, $[H_2O]_C$; beyond that, the horizontally aligned SWNTs start to be etched. In our earlier set of experiments, the $[H_2O]_C$ is between 307 and 450 ppm.

There is still another important factor in the CVD growth of SWNTs, the carbon feeding rate.[30,31] It is necessary to investigate the relationship between both growth factors (carbon feeding rate and water concentration) together to further clarify the mechanism of the selectivity. The carbon feeding rate can be controlled by changing either the concentration of carbon precursors or the concentration of hydrogen. Lower hydrogen concentration will increase the carbon feeding rate in general. Another series of growth experiments were performed using a higher carbon feeding rate by using a lower H_2 flow rate of ~280 sccm and an Ar flow rate through the water bubbler at 20 sccm (~347 ppm), 30 sccm (~508 ppm), and 45 sccm (~736 ppm). In this series of experiments, the density enhancement effect of water vapor becomes more obvious (Figure 3a–c). Compared with the sample synthesized without water vapor (Figure 1a), the SWNT density improved more than 10 times (~10 SWNT/μm) by adding a water vapor concentration of ~508 ppm (Figure 3b). The on/off ratio measurement was also used to estimate the percentages of semiconducting nanotubes in the samples. There are ~61% and ~86% devices with the on/off larger than 10 in the samples synthesized with a water vapor concentration of ~347 ppm (Figure 3d,g) and ~508 ppm (Figure 3e,h), respectively. A dramatic decrease of the array density is observed when the water vapor concentration is ~736 ppm. According to the results of electrical measurement, there is also no obvious selectivity found in this sample (Figure 3f,i).

The higher critical concentration $[H_2O]_C$ between 508 and 736 ppm in this experimental series differs from the previous result of 307–450 ppm, thus indicating that the critical concentration varies with the carbon feeding rate. The electrical measurement results show the selectivity of the samples synthesized at a higher carbon feeding rate is not as high as the samples synthesized at a lower carbon feeding rate, but higher density SWNT arrays can be obtained at a higher carbon feeding rate. Therefore, for growing a high-percentage semiconducting array, a low carbon feeding rate is essential to ensure that the growth speed of the metallic tube is not higher than the etching speed. Otherwise, the selectivity effect would be weakened. We describe this third rule as $R_{m,ETCH} \geq R_{m,GROWTH}$, where $R_{m,Growth}$ is the growth speed of metallic nanotubes. As aforementioned, $R_{m,ETCH}$ and $R_{m,GROWTH}$ can be simply assumed to be determined by the oxidant concentration and carbon feeding rate, respectively. Therefore, not only water vapor concentration but also the carbon feeding rate is important in determining the distribution of SWNT electronic

dx.doi.org/10.1021/ja3038992 | J. Am. Chem. Soc. 2012, 134, 14019–14026

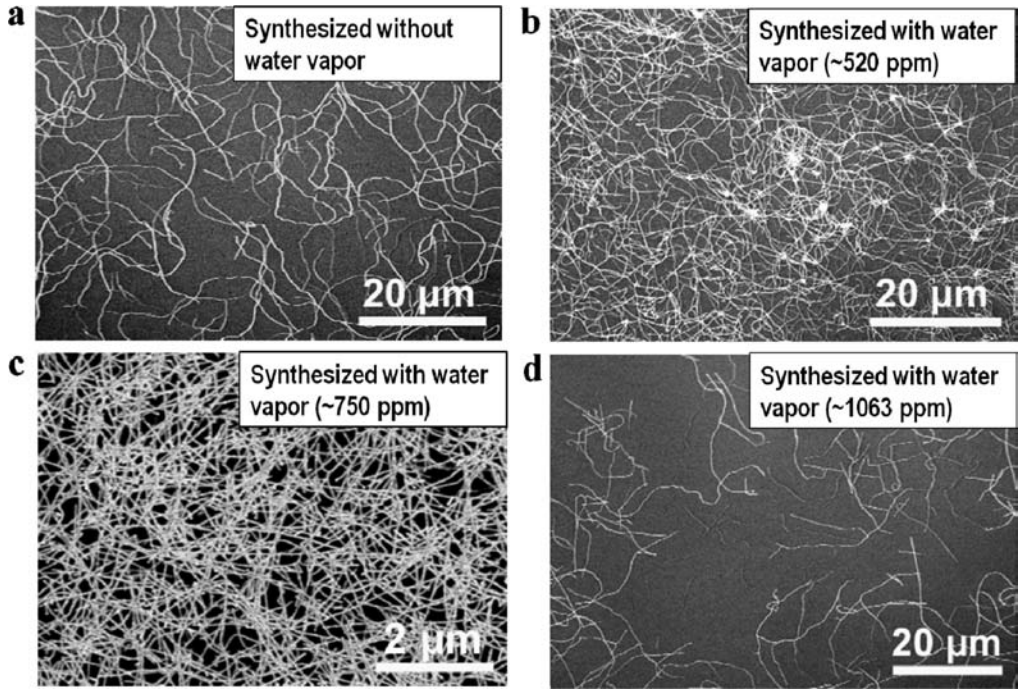

Figure 4. Water effect on the density of random SWNT network samples synthesized on silicon wafers. SEM images of the SWNT network samples synthesized without water vapor (a), with the water vapor concentration of ~520 ppm (Ar flow through water bubbler at 20 sccm) (b), ~750 ppm (Ar flow through the water bubbler at 30 sccm) (c) and ~1063 ppm (Ar flow through the water bubbler at 45 sccm) (d). The four samples were synthesized using a H_2 flow of 130 sccm and another Ar flow through the ethanol bubbler of 105 sccm.

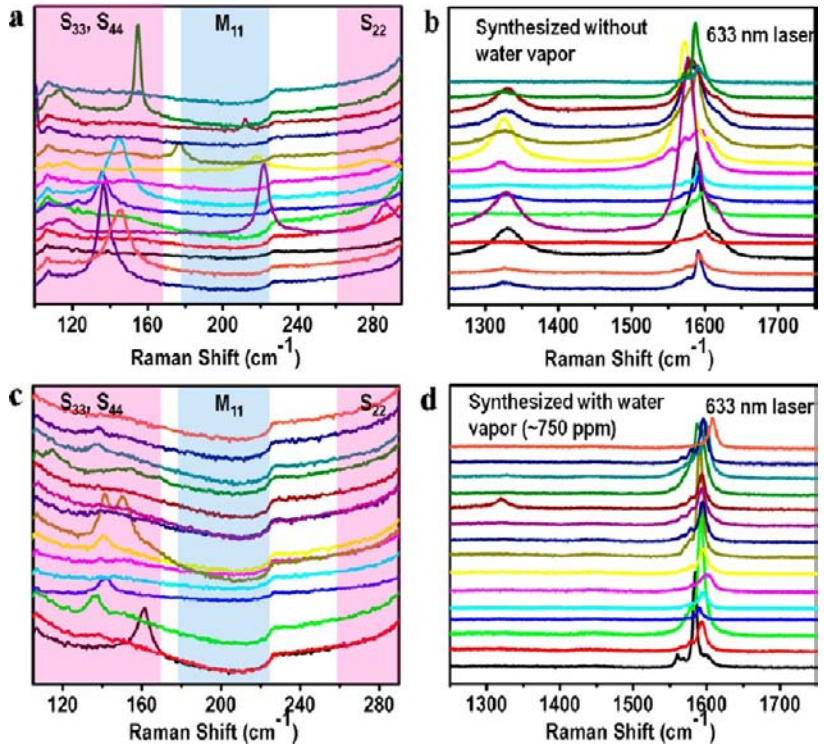

Figure 5. Raman characterizations of the SWNT network samples synthesized on silicon wafers without water vapor and with water vapor. The low-frequency (a) and high-frequency parts (b) of Raman spectra of the SWNT network sample synthesized without water vapor. The low-frequency (c) and high-frequency parts (d) of Raman spectra of the SWNT network samples synthesized with the water vapor concentration of ~750 ppm. The density of SWNT network sample synthesized with the water vapor concentration of ~1063 ppm is so low that Raman signal is hardly collected. The laser excitation wavelength of Raman spectroscopy is 633 nm. The regions corresponding to semiconducting transitions are labeled as S_{22} and $S_{33,44}$ (shaded pink), and the first-order metallic transition is labeled as M_{11} (shaded blue). The spectra were collected at 15 spots for each sample. The step at ~225 cm^{-1} originates from the silicon wafer. The laser with the wavelength excitation of 785 nm was not used for characterizing the samples because in our Raman system there is a significantly strong background signal when it is used on silicon wafers.

dx.doi.org/10.1021/ja3038992 | J. Am. Chem. Soc. 2012, 134, 14019–14026

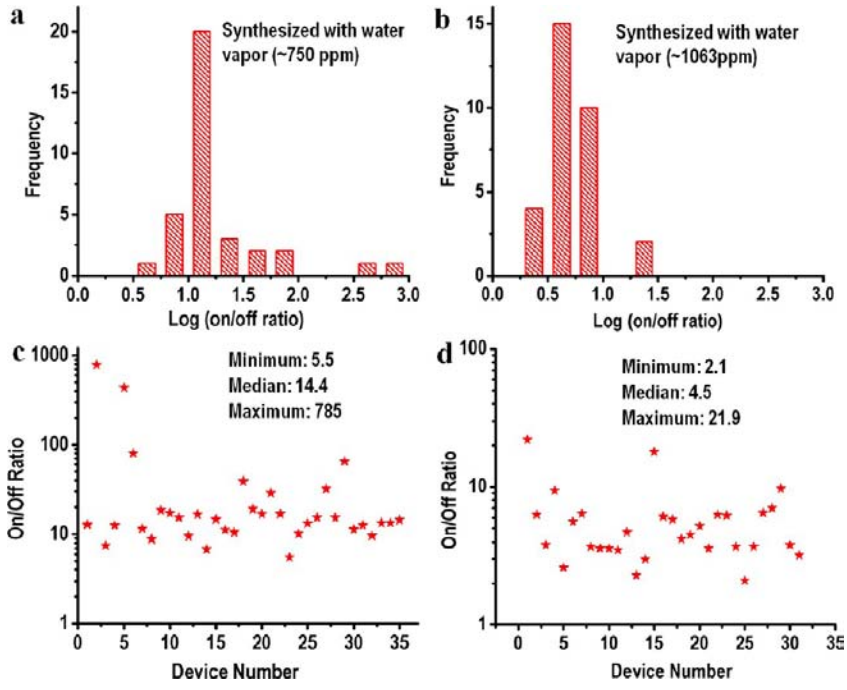

Figure 6. On/off ratio measurement results of the SWNT network samples synthesized on silicon with water vapor. Histograms of on/off ratio distributions of the TFT devices based on the network SWNT synthesized on silicon with the water vapor concentration of ~750 (a) and ~1063 ppm (b). Display of on/off ratios of all TFT devices based on the network SWNT synthesized on silicon with the water vapor concentration of ~750 (c) and ~1063 ppm (d).

types. To conclude, we summarize the three necessary rules for achieving a high selectivity in the CVD growth process:

(1) $R_{m,ETCH} > R_{s,ETCH}$: There is a suitable concentration for water vapor.

(2) $[H_2O] < [H_2O]_C$: Water vapor concentration needs to be lower than the critical concentration.

(3) $R_{m,ETCH} \geq R_{m,GROWTH}$: Use a low carbon feeding rate for high selectivity.

There is a different opinion about the water vapor etching effect on the horizontally aligned SWNTs grown on quartz wafers reported by Li et al. recently.[32] In their experimental results, there is no growth efficiency enhancement and selectivity. Contrary to our observations, an effect of preferential etching of metallic nanotubes was observed after the postgrowth water treatment. We speculate that it is due to a much higher carbon feeding rate (they used room temperature ethanol vapor and much lower total flow rate) and water concentration (around thousands ppm and horizontally aligned nanotubes were greatly etched) used in their CVD processes, which do not satisfy the rules we propose here.

Water Effect on the Growth of Random SWNT Networks on Silicon Wafers. We also tested these three general rules on silicon wafers, but discovered a higher carbon feeding rate is required for growing single-walled carbon nanotubes on silicon wafer than on quartz wafers. When H_2 flow rate was decreased to ~130 sccm and Ar flow rate through ethanol bubbler was increased to 105 sccm, a few of SWNTs started to grow on silicon wafers (Figure 4a) under the condition without water vapor. Another three samples were synthesized by maintaining this CVD condition and introducing Ar flow through water bubbler at the flow rates of ~20 sccm (~520 ppm), ~30 sccm (~750 ppm), and ~45 sccm (~1063 ppm). The density of random SWNTs on silicon wafers also shows a trend similar to that of the growth results observed on quartz wafers (Figure 4a–d).

Raman spectra show that the G band features changed from asymmetry Breit–Wigner–Fano (BWF) (Figure 5b) line shape dominating to symmetric Lorentz line shape dominating (Figure 5d) with the increase of water concentration. BWF peak is often observed in Raman spectra of metallic tubes, and Lorentz peak is the typical G band feature of semiconducting nanotubes.[22] It is interesting that the relatively high D band intensity was observed for the sample synthesized without water (Figure 5a), possibly because the high carbon feeding rate caused the formation of amorphous carbon on nanotube or wafer surface. But most of Raman spectra of the sample synthesized with ~750 ppm water vapor did not show visible D band (Figure 5d), which indicates that water vapor prefers to remove the amorphous carbon on nanotube surface and barely reacts with carbon nanotubes. At the low-frequency area of Raman spectra of the sample synthesized without water vapor, both metallic and semiconducting tubes show RBM resonance and RBM peaks observed from 80 cm^{-1} to 300 cm^{-1} (Figure 5a), indicating the SWNT sample has a broad diameter distribution. No metallic tube signal was observed in the samples synthesized with ~750 ppm water vapor (Figure 5c).

The on/off ratio measurements were performed to confirm the Raman results. For the sample synthesized with ~750 ppm water vapor, ~87% of the devices show on/off ratios larger than 10, and the median on/off ratio is 14.4 (Figure 6a,c), which is very similar to the measurement results of the sample synthesized on a quartz wafer using a higher carbon feeding rate. The density of the SWNT network sample synthesized with the water vapor concentration of ~1063 ppm is very low, and electrical measurement showed no selectivity (Figure 6b,d). Exceptionally high selectivity is difficult to achieve on a silicon wafer. We believe this is due to the higher carbon

dx.doi.org/10.1021/ja3038992 | J. Am. Chem. Soc. 2012, 134, 14019–14026

feeding rate needed for growing nanotubes on silicon wafer and it weakens the selective effect. The experimental results on silicon wafers match qualitatively with the general rules of selective growth we obtained from the growth results on the quartz wafer.

CONCLUSION

In conclusion, through the systematic investigation of the effect of water on the surface growth of SWNTs we successfully achieved a high selectivity of growing horizontally aligned nanotube arrays with a significantly enhanced fraction of semiconducting nanotubes on Y-cut quartz surfaces. The results of electrical measurements of TFTs fabricated from the as-grown samples show that over 97% of the nanotubes in the arrays are semiconducting. In addition, a density enhancement effect of SWNTs is found on quartz and silicon wafers. By exploring the relationship of water concentration and carbon feeding rate with the percentage of semiconducting in SWNT arrays grown on quartz, we proposed and verified that the selectivity originates from the etching effect of oxidants on the metallic and semiconducting nanotubes and chemical reactivity difference of metallic and semiconducting nanotubes. We proposed three general rules for achieving a high selectivity in the CVD growth process. The three rules must be simultaneously satisfied in the CVD process. Although the growth mechanism is proposed from experimental results in a water/ethanol CVD system, we believe they can be applied to other CVD system as general rules (despite the various growth conditions) and provide a possible way to obtain carbon nanotubes with predefined electronic types.

ASSOCIATED CONTENT

Supporting Information

Water concentration calculation, Raman characterization of the SWNT array samples synthesized with water and without water under the excitation of 633 nm laser, diameter measurement results of the SWNT array sample synthesized with the water concentration of ~307 ppm, schematic diagram of a ionic liquid-gated FET based on horizontally aligned SWNT array, SEM images of SWNTs on quartz synthesized with different water concentrations by CVD method, displays of on/off ratios and on-state currents of the TFT devices fabricated on the SWNT array samples synthesized with ~307 ppm water concentration and without water vapor, on/off ratio measurement results of the SWNT array sample synthesized with ~450 ppm water concentration, comparison of an as-grown SWNT array with no selectivity before and after water vapor treatment, Raman characterizations of the SWNT network samples synthesized on silicon with the water vapor concentration of ~520 ppm. This material is available free of charge via the Internet at http://pubs.acs.org.

AUTHOR INFORMATION

Corresponding Author

j.liu@duke.edu

Notes

The authors declare no competing financial interest.

ACKNOWLEDGMENTS

The work is supported in part by a grant from ONR (N00014-09-1-0163) and support from RFNano Inc. We also acknowledge the Shared Materials Instrumentation Facility (SMIF) at Duke University for access to their instrumentation. S.Z. and J.L. also acknowledge support from Lord Foundation for supporting undergraduate student in research activities.

REFERENCES

(1) Iijima, S.; Ichihashi, T. *Nature* **1993**, *363*, 603.
(2) Saito, R.; Dresselhaus, G.; Dresselhaus, M. S. Imperial College Press: London, 1998.
(3) Castro Neto, A. H.; Guinea, F.; Peres, N. M. R.; Novoselov, K. S.; Geim, A. K. *Rev. Mod. Phys.* **2009**, *81*, 109.
(4) Rutherglen, C.; Jain, D.; Burke, P. *Nat. Nanotechnol.* **2009**, *4*, 811.
(5) Koswatta, S. O.; Valdes-Garcia, A.; Steiner, M. B.; Lin, Y. M.; Avouris, P. *IEEE Trans. Microwave Theory Tech.* **2011**, *59*, 2739.
(6) Zhou, W. W.; Ding, L.; Yang, S.; Liu, J. *ACS Nano* **2011**, *5*, 3849.
(7) Wang, C. A.; Ryu, K. M.; De Arco, L. G.; Badmaev, A.; Zhang, J. L.; Lin, X.; Che, Y. C.; Zhou, C. W. *Nano Res.* **2010**, *3*, 831.
(8) Hong, S. W.; Banks, T.; Rogers, J. A. *Adv. Mater.* **2010**, *22*, 1826.
(9) Guo, J.; Hasan, S.; Javey, A.; Bosman, G.; Lundstrom, M. *IEEE Trans. Nanotechnol.* **2005**, *4*, 715.
(10) Cao, Q.; Rogers, J. A. *Adv. Mater.* **2009**, *21*, 29.
(11) Wang, C. A.; Zhang, J. L.; Zhou, C. W. *ACS Nano* **2010**, *4*, 7123.
(12) LeMieux, M. C.; Sok, S.; Roberts, M. E.; Opatkiewicz, J. P.; Liu, D.; Barman, S. N.; Patil, N.; Mitra, S.; Bao, Z. *ACS Nano* **2009**, *3*, 4089.
(13) Engel, M.; Small, J. P.; Steiner, M.; Freitag, M.; Green, A. A.; Hersam, M. C.; Avouris, P. *ACS Nano* **2008**, *2*, 2445.
(14) Rouhi, N.; Jain, D.; Burke, P. J. *ACS Nano* **2011**, *5*, 8471.
(15) Hong, G.; Zhang, B.; Peng, B. H.; Zhang, J.; Choi, W. M.; Choi, J. Y.; Kim, J. M.; Liu, Z. F. . *J. Am. Chem. Soc.* **2009**, *131*, 14642.
(16) Ding, L.; Tselev, A.; Wang, J. Y.; Yuan, D. N.; Chu, H. B.; McNicholas, T. P.; Li, Y.; Liu, J. *Nano Lett.* **2009**, *9*, 800.
(17) Wang, Y.; Liu, Y. Q.; Li, X. L.; Cao, L. C.; Wei, D. C.; Zhang, H. L.; Shi, D. C.; Yu, G.; Kajiura, H.; Li, Y. M. *Small* **2007**, *3*, 1486.
(18) Yu, B.; Liu, C.; Hou, P. X.; Tian, Y.; Li, S. S.; Liu, B. L.; Li, F.; Kauppinen, E. I.; Cheng, H. M. . *J. Am. Chem. Soc.* **2011**, *133*, 5232.
(19) Hata, K.; Futaba, D. N.; Mizuno, K.; Namai, T.; Yumura, M.; Iijima, S. *Science* **2004**, *306*, 1362.
(20) Yamada, T.; Maigne, A.; Yudasaka, M.; Mizuno, K.; Futaba, D. N.; Yumura, M.; Iijima, S.; Hata, K. *Nano Lett.* **2008**, *8*, 4288.
(21) Ding, L.; Yuan, D. N.; Liu, J. *J. Am. Chem. Soc.* **2008**, *130*, 5428.
(22) Dresselhaus, M. S.; Dresselhaus, G.; Saito, R.; Jorio, A. *Phys. Rep.* **2005**, *409*, 47.
(23) Okimoto, H.; Takenobu, T.; Yanagi, K.; Miyata, Y.; Shimotani, H.; Kataura, H.; Iwasa, Y. *Adv. Mater.* **2010**, *22*, 3981.
(24) Ye, J. T.; Craciun, M. F.; Koshino, M.; Russo, S.; Inoue, S.; Yuan, H. T.; Shimotani, H.; Morpurgo, A. F.; Iwasa, Y. *Proc. Natl. Acad. Sci. U.S.A.* **2011**, *108*, 13002.
(25) Ye, J. T.; Inoue, S.; Kobayashi, K.; Kasahara, Y.; Yuan, H. T.; Shimotani, H.; Iwasa, Y. *Nat. Mater.* **2010**, *9*, 125.
(26) Franklin, A. D.; Wong, H. S. P.; Lin, A.; Chen, Z. H. *IEEE Electron Device Lett.* **2010**, *31*, 644.
(27) Yoshihara, N.; Ago, H.; Tsuji, M. *J. Phys. Chem. C* **2007**, *111*, 11577.
(28) Lu, J.; Nagase, S.; Zhang, X. W.; Wang, D.; Ni, M.; Maeda, Y.; Wakahara, T.; Nakahodo, T.; Tsuchiya, T.; Akasaka, T.; Gao, Z. X.; Yu, D. P.; Ye, H. Q.; Mei, W. N.; Zhou, Y. S. *J. Am. Chem. Soc.* **2006**, *128*, 5114.
(29) Feng, X. F.; Chee, S. W.; Sharma, R.; Liu, K.; Xie, X.; Li, Q. Q.; Fan, S. S.; Jiang, K. L. *Nano Res.* **2011**, *4*, 767.
(30) Lu, C. G.; Liu, J. *J. Phys. Chem. B* **2006**, *110*, 20254.
(31) Qi, H.; Yuan, D. N.; Liu, J. *J. Phys. Chem. C* **2007**, *111*, 6158.
(32) Li, P.; Zhang, J. *J. Mater. Chem.* **2011**, *21*, 11815.